Fault-Tolerant Control of Wind Turbines: A Benchmark Model

Peter Fogh Odgaard, *Member, IEEE*, Jakob Stoustrup, *Senior Member, IEEE*, and Michel Kinnaert, *Member, IEEE*

***Abstract*— This paper presents a test benchmark model for the evaluation of fault detection and accommodation schemes. This benchmark model deals with the wind turbine on a system level, and it includes sensor, actuator, and system faults, namely faults in the pitch system, the drive train, the generator, and the converter system. Since it is a system-level model, converter and pitch system models are simplified because these are controlled by internal controllers working at higher frequencies than the system model. The model represents a three-bladed pitch-controlled variable-speed wind turbine with a nominal power of 4.8 MW. The fault detection and isolation (FDI) problem was addressed by several teams, and five of the solutions are compared in the second part of this paper. This comparison relies on additional test data in which the faults occur in different operating conditions than in the test data used for the FDI design.**

***Index Terms*— Benchmark modeling, fault detection, fault isolation, fault-tolerant control (FTC), wind turbines.**

I. Introduction

TODAY, wind turbines contribute to a large part of the world's power production. At the same time, the size of the standard turbine tends to increase as well. Turbines in the megawatt size are expensive, and hence their reliability is expected to be high to generate as much energy as possible. These wind turbines are expected to produce energy with very short downtimes. A way to ensure this consists in introducing advanced fault detection, isolation, and accommodation systems into the turbines. In the state-of-the-art industrial wind turbines, fault detection schemes are simple and are often conservative, and so is the fault accommodation mechanism. Turbines are turned off even during simple faults to wait for service. [In addition to the fault detection and isolation (FDI) systems, condition monitoring is used for the rotating parts.] Consequently, there is a need to use advanced fault detection, isolation, and accommodation schemes in order to improve the on-time of the turbine, even though that might result in limited power production for some faults. Some work has been performed on fault detection, isolation, and accommodation on wind turbines, but they only cover parts of the wind turbine and do not include comparisons of the performance of different schemes for the detection of faults in the various parts of the turbine.

In [1], a Kalman-filter-based diagnosis system to detect faults in the blade root bending moment sensors was presented. An unknown input observer was designed for the detection of sensor faults around the wind turbine drive train in [2]. In [3], active and passive fault-tolerant control (FTC) schemes were applied to a wind turbine model. More focus has been placed on the electrical conversion system in the wind turbines; some relevant examples can be found in [4] and [5]. In the former, an observer-based solution for current sensor fault detection is presented, whilst the latter presents a similar solution for voltage sensor fault detection. In [6], a fault detection and reconfiguration solution for handling faults in a doubly fed wind turbine converter is presented.

Comparing the various detection and accommodation schemes on the wind turbine application is beneficial in the process to find the best schemes to handle the different faults. However, since a wind turbine is a large and complex system, such a comparison can only be performed on a limited set of possible faults. In order to test various detection, isolation, and accommodation schemes on the wind turbine application, this paper presents a benchmark model of a wind turbine at the system level, containing sensor, actuator, and systems faults. This benchmark model describes a realistic generic three-blade horizontal variable-speed wind turbine with a full-scale converter coupling. This generic turbine has a rated power at 4.8 MW. Since this model works at the system level, the fast control loops of the converters are not considered.

This wind turbine FDI and FTC benchmark model was originally presented in [7]. The purpose of this benchmark was to provide a model on which researchers working in the field of fault diagnosis and fault-tolerant control can compare different methods in their field applied to a wind turbine. Wind turbines are complicated machines; it was therefore decided to keep the benchmark model simple so that non wind-turbine experts can use it. Consequently, some simplifications and assumptions are made. Blades and tower are assumed rigid, and aerodynamics are described by a static model. The wind turbine controller included in the model is also simple, leaving out some typical features; however, it controls the wind turbine with acceptable performance. In this paper, the model is extended with even more faults and test sets, and is described in more detail, so that a better understanding of the benchmark model is provided. Additional test sets are introduced to test

Manuscript received December 2, 2011; revised September 19, 2012 and January 29, 2013; accepted March 26, 2013. Manuscript received in final form April 18, 2013. Date of publication May 22, 2013; date of current version June 14, 2013. The work of P. F. Odgaard was supported by kk-Electronic a/s. Recommended by Associate Editor G. E. Stewart.

P. F. Odgaard and J. Stoustrup are with Aalborg University, Aalborg 9220, Denmark (e-mail: pfo@es.aau.dk; jakob@es.aau.dk).

M. Kinnaert is with the Department of Control Engineering and System Analysis, Université libre de Bruxelles, Bruxelles 1050, Belgium (e-mail: michel.kinnaert@ulb.ac.be).

Color versions of one or more of the figures in this paper are available online at http://ieeexplore.ieee.org.

Digital Object Identifier 10.1109/TCST.2013.2259235

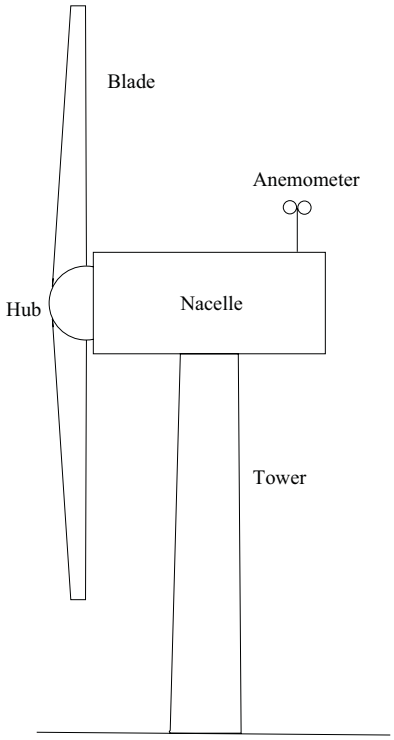

Fig. 1. General outline of the wind turbine seen from the outside.

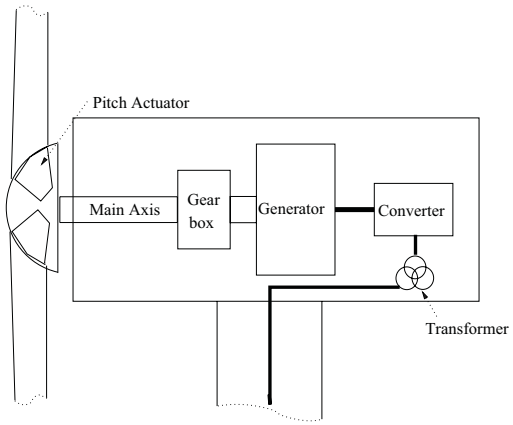

Fig. 2. Major parts from inside of the nacelle. It can be seen that the blades are fixed to the main axis, which in turn is connected to the generator through the gear box. The generator is electrically connected to the converter, which in turn is connected to a transformer. The blades are pitched by the pitch actuators.

the robustness of solutions toward different points of operation at which faults are introduced. This paper also presents some of the best FDI solutions applied to this benchmark model. In these tests, an internal model from kk-electronic a/s is used, which includes some additional model features to test further robustness of the proposed schemes. The compared solutions can be seen in [8]–[12]. These solutions are evaluated and compared based on the requirements in the benchmark statement. Experiences gained by usage of the methods on the benchmark are provided as well. A number of other solutions have also been applied to this benchmark model. Among these are [13]–[27].

The rest of this paper is organized as follows. In Section II, the functionality of wind turbines is described; the fault scenarios are presented in Section III. Next, in Section IV, the wind turbine model is presented. In Section V, the test signals are characterized. The different FDI solutions considered and compared in this paper are introduced in Section VI. These solutions are compared in Section VII. Conclusions are drawn in Section VIII.

II. Wind Turbine Description

Wind turbines generate electrical energy from the kinetic energy in the wind. In this test bench model, a specific kind of turbine is considered. This turbine is a three-blade horizontal-axis turbine with a full converter coupling, even though, at this system level, the difference is small between a full converter and a doubly fed induction generator. Both these generator types are variable-speed and pitch-controlled turbines. More details on wind turbine generator types can be found in [28] and [29]. The physical outline of the wind turbine is shown in Fig. 1, from which it can be seen that the nacelle is mounted at the top of a tower. Inside the nacelle lies the control equipment and the equipment to convert energy from the rotating mechanical system to electrical energy. The blades are fixed to the main axis (not seen in the figure) in the hub. The anemometer is placed on the top of the nacelle and measures the wind speed and direction. Fig. 2 represents the interior of the nacelle, showing that the main axis is connected to the generator through a gear box; the generator is connected to the grid through the converter and a high-voltage transformer. The general functioning starts with pressure from the wind on the turbine blades, forcing the wind turbine rotor to spin around. Energy is converted from kinetic wind energy to mechanical energy through a rotating shaft. This energy generation can be controlled by changing the aerodynamics of the rotor. This is achieved by pitching the blades or by controlling the rotational speed of the rotor relative to the wind speed. Mechanical energy is converted to electrical energy by a generator coupled to a converter with rating equal to the rated power of the generator. Between the rotor and the generator, a gear box is used to transform the rotational speed from the rotor to the generator. The converter can be used to set the generator torque, which consequently can be used to control the rotational speed of the generator as well as the rotor. A more detailed description of the general functioning of the wind turbine can be seen in [28]–[30].

The objective of the control system is to follow the power reference. In case the wind speed is too low for the wind turbine to reach the power reference, the controller will try to optimize the power production. This power control should keep the mechanical vibrations at an acceptable level. A system overview can be seen in Fig. 3. This figure shows the relations between the blade and the pitch system, the drive train, the generator and converter, and the controller. The variables between these subsystems are defined as follows: v_{w} is the wind speed acting on the turbine blades; τ_{w} is the torque from the wind acting on the turbine blades; τ_{r} is the rotor torque; ω_{r} is the rotational speed of the rotor; τ_{g} is the generator torque; ω_{g} is the rotational speed of the

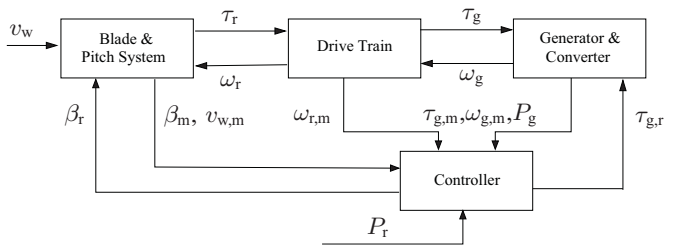

Fig. 3. Overview of the benchmark model. It consists of four parts: blade and pitch systems, drive train, generator and converter, and controller. The variables in the figure are defined in the text.

generator; β_r is the reference to the pitch position; β_m is the measured pitch position; $\tau_{w,m}$ is an estimated wind torque based on wind speed measurement; $\omega_{r,m}$ is the measured rotational speed of the rotor, $\omega_{g,m}$ is the measured rotational speed of the generator; $\tau_{g,m}$ is the measured generator torque; $\tau_{g,r}$ is the torque reference to the generator; P_r is the power reference to the wind turbine; and P_g is the power produced by the generator. The wind turbine controller provides three pitch references, and all three pitch positions are measured with two sensors to ensure physical redundancy of the pitch position measurements. The generator and rotor speeds are also measured with two sensors each for the same reason. These variables are defined as β_{r1}, β_{r2}, and β_{r3} for the pitch reference to blades 1, 2, and 3. $\beta_{1,m1}$ and $\beta_{1,m2}$ are the two pitch measurements for blade 1; $\beta_{2,m1}$ and $\beta_{2,m2}$ are the two pitch measurements for blade 2; and $\beta_{3,m1}$ and $\beta_{3,m2}$ are the two pitch measurements for blade 3. The two rotor speed measurements are defined as $\omega_{r,m1}$ and $\omega_{r,m2}$; the two generator speed measurements are defined as $\omega_{g,m1}$ and $\omega_{g,m2}$.

A. Control System Concept

The controller operates in principle in four operational zones governed by the mean wind speed within some time window. These control zones are plotted depending on the wind speed in Fig. 4. In zone 1, the turbine is at standstill; zone 2 is power optimization or partial load; zone 3 is constant power production; zone 4 is high wind speed. In zone 4, the turbines are pitched out of the wind to stop the rotation and the energy production of the turbine. Zones 1 and 4 are not considered any further in this paper and are excluded from the benchmark model, since the focus is on detecting faults under normal operations, which are covered by zones 2 and 3 [31]. An extra control zone is often used between zones 2 and 3, providing a smoother transition between the control zones and placing lower structural loads on the wind turbine. This will influence the FDI scheme working on the wind turbine, since there is a correlation between FDI and the controls of the wind turbine. However, the proposed control structure gives a more challenging detection and isolation problem since larger transients are present. Therefore this simple control structure is relevant in the benchmark model.

In Fig. 4, the power curve for the wind turbine is plotted. This figure shows that for wind speeds between 0 and 12.5 m/s the turbine is controlled to obtain optimal power production. The optimal power is obtained when the pitch angle of the blade β is equal to 0 degrees, and the tip speed ratio is kept constant at its optimal value. The tip speed ratio λ is defined as

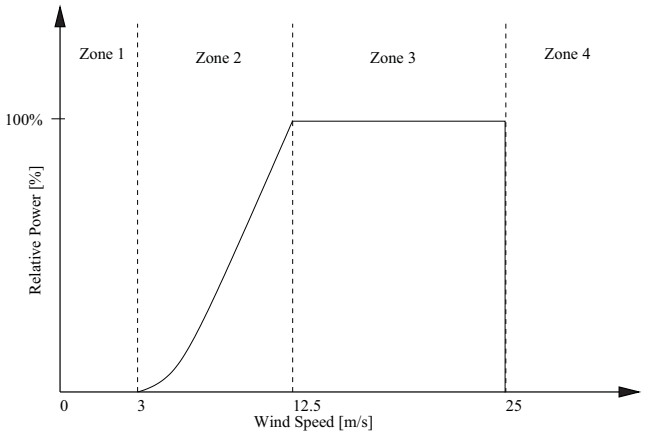

Fig. 4. Illustration of the reference power curve for the wind turbine depending on the wind speed. In zone 1, the wind turbine will be idling awaiting higher wind speeds (0–3 m/s). In zone 2, the generated power of the wind turbine will be optimized (3–12.5 m/s). In zone 3, the wind turbine will be controlled to keep a constant power generation (12.5–25 m/s). In zone 4, the wind turbine will be parked, preventing damage due to the high wind speed (above 25 m/s).

$$\lambda = \frac{\omega_r \cdot R}{v_w} \tag{1}$$

where R is the radius of the blades, and v_w is the wind speed. The optimal power curve is followed by controlling the generator torque reference $\tau_{g,r}$ to its optimal value.

When the nominal power reference is achieved, the controller is switched to control zone 3. In this zone, the control objective is to maintain the power reference P_r. This objective is obtained by controlling β_r, such that the power coefficient of the wind turbine C_P is decreased. In an industrial control scheme, a proportional integral (PI) controller is often used to keep ω_r at the rated value by changing β_r.

More details on the wind turbine controller can be found in Section IV-E.

III. Fault Scenarios

In this benchmark model, some faults are considered. These faults cover sensor, actuator, and process faults in different parts of the wind turbine. In the following, these different kinds of faults are listed. These faults have various degrees of severity. Some are very serious and must result in a fast and safe closing down of the wind turbine. The rest are less severe in the sense that the controller can accommodate these faults while staying in operation, possibly with a reduced performance. Both additive and multiplicative faults as well as faults resulting in changed dynamics of parts of the system are considered in this benchmark model. The faults are chosen to cover different kinds of faults so they require different qualities in the FDI and FTC schemes. All the described faults originate from actual faults in wind turbines, but the details of the actual faults cannot be presented for confidentiality reasons. To sum up, the faults are selected to cover different parts of the wind turbine, different fault types and classes, and different levels of severity.

A. Sensor Faults

Some of the more relevant faults are considered in this benchmark model. The first is a fault in the pitch position measurements. These faults are denoted $\Delta\beta_{1,\mathrm{m1}}$, $\Delta\beta_{1,\mathrm{m2}}$, $\Delta\beta_{2,\mathrm{m1}}$, $\Delta\beta_{2,\mathrm{m2}}$, $\Delta\beta_{3,\mathrm{m1}}$, and $\Delta\beta_{3,\mathrm{m2}}$. The origin of these faults is either electrical or mechanical faults in the position sensors, and can result in either a fixed value or a changed gain factor on the measurements. These two fault types are considered since they have been seen in wind turbines and it is important to detect and accommodate these kinds of faults. Especially, the fixed value should be easy to detect, and therefore it is important that a fault detection, isolation, and accommodation scheme be able to deal with this fault. If not handled correctly, these faults will influence the pitch positions because the internal controller in the pitch system controls the pitch positions based on these pitch position measurements.

Secondly, the rotor speed measurement can be faulty. We denote the deviations in rotor speed measurement caused by these faults as $\Delta\omega_{\mathrm{r,m1}}$ and $\Delta\omega_{\mathrm{r,m2}}$. The fault signals for the two generator speed measurements are denoted as $\Delta\omega_{\mathrm{g,m1}}$ and $\Delta\omega_{\mathrm{g,m2}}$. Both the rotor and generator speed measurements are done using encoders. Encoder faults can be due to both electrical and mechanical failures, which result in either a fixed value or a changed gain factor on the measurements. In case of a fixed value fault, the output of the encoder is not updated with new values. The gain factor fault is introduced when the encoder reads more marks on the rotating part than actually present, which can happen as a result of dirt or other false markings on the rotating part.

B. Actuator Faults

Both the converter and pitch systems can be faulty. Converter faults are denoted as $\Delta\tau_{\mathrm{g}}$ and can result in either an offset or in changed dynamics of the converter. The cause of this fault is internal to the converter, and is due to either a fault in the converter electronics or an off-set on the converter torque estimate. The converter controller would typically be able to detect the faults in the electronics, but the converter torque offset is difficult to detect internally. Yet, from a wind turbine level, it is possible to detect, isolate, and accommodate a torque offset because it changes the torque balance in the wind turbine power train.

The pitch system, which in this case is hydraulic, has the possibility of faults on all three blades, and these faults are denoted as $\Delta\beta_1$, $\Delta\beta_2$, and $\Delta\beta_3$. Faults in the pitch system are considered in the hydraulic system, which can result in changed dynamics due to either a drop in pressure in the hydraulic supply system or high air content in the oil. The former represents faults such as a leakage in hose, a blocked pump, or similar others. There will always be some air content in the hydraulic oil used, the content level will vary, and it is not possible to control it well. Air is much more compressible than oil, so it changes the dynamics of the hydraulic actuator.

C. System Faults

The considered system fault is found in the drive train, where the friction coefficient in the model changes slowly with time. This change will result in two correlated fault signals: $\Delta\omega_{\mathrm{r}}$ and $\Delta\omega_{\mathrm{g}}$. These changes evolve slowly in reality; however, it is expected to be too demanding in the benchmark simulator from a computational point of view to simulate such a fault realistically evolving over a period of months or even years. Consequently, in this benchmark model, this fault is represented by a small change of the friction coefficient within a few seconds. The main point is that the change in the drive train friction is much slower than the system dynamics and the system sample rate. Typically, faults in wind turbine gear boxes are found using condition monitoring methods relying on additional sensors that measure accelerations, noise levels, etc., on the gear box; an extensive review of this can be found in [32]. It would be more cost efficient if such faults could be detected and isolated using standard measurement in the wind turbine control system; this fault is therefore included in the benchmark.

D. Severity of Faults

All the faults mentioned above are summarized and listed in Table I. In this table, fault details such as the type, consequence, severity, and developing time are given. Notice also that the letter in the fault class indicates a sensor (A), actuator (B), or system fault (C).

In order to deal with these faults in a prioritized order, the severity and consequences of these considered faults, as well as the time of development of the faults, are listed in Table I. Notice that the severity level of all these sensor faults is set low because of the physical redundancy of the sensors, so sensor faults are not a problem when they are detected fast and the sensor systems are reconfigured. However, when these faults are not handled, they are critical. Notice that the changed dynamics of the drive train, due to increased friction, is not that severe, but should be detected as an indication of the wear of the drive train. However, over the years this wear and tear of the drive train will accumulate, leading to a total breakdown of the drive train, which clearly is a highly severe fault, since it is not only highly costly to replace but it also results in a long downtime of the wind turbine as a consequence.

E. Fault Detection and Isolation Requirements

The FDI requirements are listed in this subsection. The detection time T_{D} for the respective faults is defined in terms of the sampling time for the control system T_{s}, which, in this case, is equal to 0.01 s.

1) Time of Detection: The maximum detection times for all faults are provided in the following. The respective fault amplitudes are taken into account in the selection of these detection requirements. The requirements are set such that faults have not yet developed into critical faults, but also such that detection and isolation is challenging considering the fault amplitude. All the sensor faults are required to fulfill $T_{\mathrm{D}} < 10 \cdot T_{\mathrm{s}}$. For the converter faults, the requirement is $T_{\mathrm{D}} < 3 \cdot T_{\mathrm{s}}$. For the pitch system fault, due to dropped pump pressure (fault B3), $T_{\mathrm{D}} < 8 \cdot T_{\mathrm{s}}$ is required to hold, and for air in the oil (fault B4), $T_{\mathrm{D}} < 100 \cdot T_{\mathrm{s}}$ is required. An increased

TABLE I
FAULTS CONSIDERED IN THE BENCHMARK MODEL INCLUDING FAULT TYPES, SEVERITY, AND TIME OF DEVELOPMENT OF THE CONSIDERED FAULTS

Fault class	Fault	Type	Symbols	Consequence	Severity	Dev. Time
A1	Sensor fault	Fixed value	$\Delta\beta_{1,\mathrm{m1}}$, $\Delta\beta_{1,\mathrm{m2}}$, $\Delta\beta_{2,\mathrm{m1}}$, $\Delta\beta_{2,\mathrm{m2}}$, $\Delta\beta_{3,\mathrm{m1}}$, $\Delta\beta_{3,\mathrm{m2}}$	False measurement, reconfigure system	Low	Medium
A2	Sensor fault	Gain factor	$\Delta\beta_{1,\mathrm{m1}}$, $\Delta\beta_{1,\mathrm{m2}}$, $\Delta\beta_{2,\mathrm{m1}}$, $\Delta\beta_{2,\mathrm{m2}}$, $\Delta\beta_{3,\mathrm{m1}}$, $\Delta\beta_{3,\mathrm{m2}}$	False measurement, reconfigure system	Low	Medium
A3	Sensor fault	Fixed value	$\Delta\omega_{\mathrm{r,m1}}$, $\Delta\omega_{\mathrm{r,m2}}$	False measurement, reconfigure system	Low	Medium
A4	Sensor fault	Gain factor	$\Delta\omega_{\mathrm{r,m1}}$, $\Delta\omega_{\mathrm{r,m2}}$	False measurement, reconfigure system	Low	Medium
A5	Sensor fault	Fixed value	$\Delta\omega_{\mathrm{g,m1}}$, $\Delta\omega_{\mathrm{g,m2}}$	False measurement, reconfigure system	Low	Medium
A6	Sensor fault	gain Factor	$\Delta\omega_{\mathrm{g,m1}}$, $\Delta\omega_{\mathrm{g,m2}}$	False measurement, reconfigure system	Low	Medium
B1	Actuator fault	Changed dynamics	$\Delta\tau_{\mathrm{g}}$	Slow torque control, indicates serious problems	High	Fast
B2	Actuator fault	Offset	$\Delta\tau_{\mathrm{g}}$	None optimal power production	Medium	Fast
B3	Actuator fault	Changed dynamics	$\Delta\beta_1$, $\Delta\beta_2$, $\Delta\beta_3$ (Hydraulics)	Problems with pump or leakage, slow control actions	High	Medium
B4	Actuator fault	Changed dynamics	$\Delta\beta_1$, $\Delta\beta_2$, $\Delta\beta_3$ (Air in oil)	Air in oil, slow control actions	Medium	Slow
C1	System fault	Changed dynamics	$\Delta\omega_{\mathrm{r}}$, $\Delta\omega_{\mathrm{g}}$	Increased level of drive train vibrations	Medium	Very slow

drive train friction is just expected to be detected with no specific time requirement. It is recommended that Monte Carlo studies be applied to test that the detection scheme can detect the respective faults with these requirements. One hundred simulation runs should be performed, with different measurement noise realizations.

2) False Detections: The number of false detections is required to be kept low, and the interval between false detections is required to be larger than 100 000 samples on average. The false detections must last for no more than three samples. This number corresponds to 4.4 faults on average per simulated test series; consequently, a Monte Carlo study with 100 repetitions will allow 440 false detections in total.

3) Missed Detections: The faults included in this benchmark model are of such a size that they all should be detected.

4) Issues to be Aware of: A major problem in the wind turbine control system in general is that, seen from a control theoretical point of view, the wind turbine is driven by a disturbance, namely the wind. The wind speed is, however, measured to some extent with significant measurement noises added as well as a large risk of an offset. This offset can be calibrated, but it is recommended to be considered in the FDI system. The measurement noise is modeled as a Gaussian white noise, for which the parameters can be found in the list of parameters (Table VII).

It is important to notice the nonlinearities in the aerodynamics of the turbine as well as the switching control structure. The FDI system is expected to be robust toward uncertainties in this aerodynamic model, partly because exact measures of this mapping on the specific turbines are difficult. This aerodynamic mapping might also change with time because of debris buildup on the blades. For more information on this specific problem, consult [31], [33], and [34].

F. Accommodation Requirements

The benchmark model of this paper contains both faults for which the system can be reconfigured to continue power generation and very severe faults that require a safe and fast shutdown of the wind turbine. The last group contains the severe faults in the two actuators with fault numbers B1 and B3. All remaining faults must be accommodated in some way, and the wind turbine must continue its operation. In all cases, detection of faults must be reported to the system operator, and automatic action is required. In case of a single sensor fault, system performance must not deteriorate; in the case of multiple faults, a mild deterioration of the system performance is accepted. Large transients when accommodating the fault must be avoided.

In order to evaluate the power generation during a fault, a power generation error sum $\sum P_{\mathrm{e}}$ is defined in

$$\sum P_{\mathrm{e}} = \sum_{n \in N} \left(P_{\mathrm{g}}[n] - P_{\mathrm{r}}[n]\right)^2 \tag{2}$$

where N is the number of samples in a given faulty mode. $\sum P_{\mathrm{g}}$ for the faulty case should be as close as possible to the fault-free case. In addition, two constraints should not be violated, i.e., $P_{\mathrm{g}}[n] < 1.1 \cdot 4.8$ [MW], and $\omega_{\mathrm{g}}[n] < 1.1 \cdot \omega_{\mathrm{nom}}$, where ω_{nom} is given in Table VI. The maximum allowed power is given by the generator and converter design, and the maximum allowed value of $\omega_{\mathrm{g}}[n]$ is given by structural considerations.

IV. Wind Turbine Model

In this section, the various model parts are presented according to the following order: wind model, blade and pitch model, drive train model, generator/converter model, and controller. Finally, the numerical values of the different parameters are indicated. Notice here that the benchmark model implemented in Simulink can be downloaded by the URL address http://www.kk-electronic.com/wind-turbine-control/competition-on-fault-detection/wind-turbine-benchmark-model.aspx [35].

A. Wind Model

In this benchmark model, a wind model is included that describes stochastic wind behavior as well as wind shear effects (namely variations in the wind speed depending of height) and tower shadow effects (accounting for the passing of the blade in front of the wind turbine tower). Such a model can be found in [36]. This implementation is used in the benchmark model. The model will be presented in this paper without much explanation since the derivation of the parts can be found in the references. This wind model consists of four parts: the mean wind (slow wind variations) $v_{\mathrm{m}}(t)$; a stochastic part $v_{\mathrm{s}}(t)$; the wind shear $v_{\mathrm{ws}}(t)$ (which is the effect of wind energy lost at the surface of the earth, resulting normally in an increasing wind speed as the distance to the earth surface increases); and the tower shadow $v_{\mathrm{ts}}(t)$. The combined wind model is given by

$$v_{\mathrm{w}}(t) = v_{\mathrm{m}}(t) + v_{\mathrm{s}}(t) + v_{\mathrm{ws}}(t) + v_{\mathrm{ts}}(t). \tag{3}$$

In this benchmark model, four different wind speeds are required: the wind speed at hub height as measured by the anemometers and three speeds at the three blade tips, respectively, denoted as $v_{\mathrm{hub}}(t)$, $v_{\mathrm{w1}}(t)$, $v_{\mathrm{w2}}(t)$, and $v_{\mathrm{w3}}(t)$. The last three are altered by the wind shear and the tower shadow, while the first is not. Consequently, $v_{\mathrm{hub}}(t)$ only depends on the first two terms in (3), while the three blade wind speeds vary according to their angular position in the rotor plane.

In terms of mean wind, a slowly varying wind sequence is obtained by processing a set of measured wind data with a low-pass filter. The stochastic part of the wind model is modeled by Kaimal filters (see [30] for details and [37] for implementation details). An implementation of this model can be found in the Simulink implementation of this benchmark model [35].

The wind shear model is given by

$$v_{\mathrm{ws},i}(t) = \frac{2v_{\mathrm{m}}(t)}{3\cdot R^2}\cdot\left(\frac{R^3\cdot\alpha}{3\cdot H}\chi + \frac{R^4}{4}\cdot\alpha\cdot\frac{\alpha-1}{2\cdot H^2}\cdot\chi^2\right) + \frac{2v_{\mathrm{m}}(t)}{3\cdot R^2}\cdot\left(\frac{R^5}{5}\cdot\frac{(\alpha^2-\alpha)\cdot(\alpha-2)}{6\cdot H^3}\cdot\chi^3\right) \tag{4}$$

where $\chi = \cos(\theta_{\mathrm{r}*}(t))$, and $\theta_{\mathrm{r}*}$ is the angular position of the three blades, $\theta_{\mathrm{r1}}(t) = \theta_{\mathrm{r}}(t)$, $\theta_{\mathrm{r2}}(t) = \theta_{\mathrm{r}}(t) + (2/3)\pi$, and $\theta_{\mathrm{r3}} = \theta_{\mathrm{r}}(t) + (4/3)\pi$. α and H used in (4) are two aerodynamic parameters.

The tower shadow model is given by

$$v_{\mathrm{ts},i}(t) = \frac{m\cdot\bar{\theta}_{\mathrm{r},i}(t)}{3\cdot r^2}\cdot(\psi + v)$$

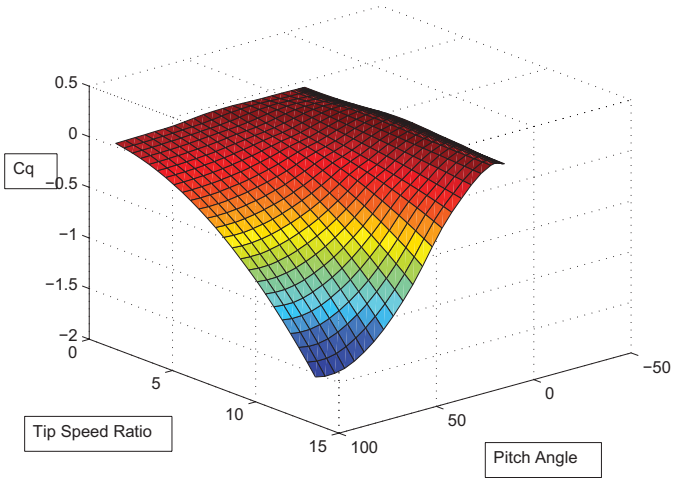

Fig. 5. Torque coefficient C_{q} as a function of the tip speed ratio λ and the pitch angle β.

where

$$\psi = 2a^2\frac{R^2 - r_0^2}{(R^2 + r_0^2)\sin(\bar{\theta}_{\mathrm{r},i}(t))^2 + k^2)}$$

$$v = 2a^2k^2\frac{(r_0^2 - R^2)(r_0^2\sin(\bar{\theta}_{\mathrm{r},i}(t))^2 + k^2)}{R^2\sin(\bar{\theta}_{\mathrm{r},i}(t))^2 + k^2}$$

$$m = 1 + \frac{\alpha\cdot(\alpha-1)\cdot r_0^2}{8\cdot H^2}$$

$$\bar{\theta}_{\mathrm{r},i}(t) = \theta_{\mathrm{r}}(t) + \frac{(i-1)\cdot 2\pi}{3} - \mathrm{floor}\left(\frac{\theta_{\mathrm{r}}(t) + \frac{(i-1)\cdot 2\pi}{3}}{2\pi}\right)\cdot 2\pi$$

and the function floor(x) is the largest integer not greater than x, r_0 is the radius of the blade hub, and k is an aerodynamic parameter.

B. Blade and Pitch Model

This model is a combination of the aerodynamic model and the wind and pitch model. τ_{r} is found using the aerodynamic model, which requires inputs from the wind and pitch models.

1) Aerodynamic Model: The aerodynamics of the wind turbine is modeled as a torque acting on the blades. This aerodynamic torque can be represented by the following expression [31]:

$$\tau_{\mathrm{r}}(t) = \frac{\rho\pi R^3 C_{\mathrm{q}}(\lambda(t),\beta(t))v_{\mathrm{w}}(t)^2}{2} \tag{5}$$

in which $C_{\mathrm{q}}(\lambda(t),\beta(t))$ is a mapping of the torque coefficients depending on the tip speed ratio and the pitch angle. The C_{q} mapping used in this model can be seen in Fig. 5. In order to model the three blades to have their own pitch angle value, a simple model is used. The latter assumes that the torque of each blade is equal to a third of the torque given by the three blades. Consequently, the aerodynamic torque equation becomes

$$\tau_{\mathrm{r}}(t) = \Sigma_{1\le i\le 3}\frac{\rho\pi R^3 C_{\mathrm{q}}(\lambda(t),\beta_i(t))v_{\mathrm{w},i}(t)^2}{6}.$$

This model is valid for small differences between the pitch angles. A more detailed model has shown similar behavior.

2) Pitch System Model: The hydraulic pitch system is modeled as a closed-loop transfer function between the measured pitch angle β_{m} and its reference β_{ref}. β_{ref} is the input to the closed-loop transfer function and it is provided by the wind turbine controller; β_{m} is the output of the transfer function which is also the measurement used by the internal pitch actuator controller. β_{m} is available for the wind turbine control system and therefore also for FDI and FTC schemes. Notice that the control signal from the internal pitch actuator controller is not available. In principle, it is a piston servo system that can be modeled well by a second-order transfer function [38]

$$\frac{\beta(s)}{\beta_{\mathrm{r}}(s)} = \frac{\omega_{\mathrm{n}}^2}{s^2 + 2 \cdot \zeta \omega_{\mathrm{n}} \cdot s + \omega_{\mathrm{n}}^2} \tag{6}$$

where ζ is the damping factor, and ω_{n} is the natural frequency. A transfer function is attached to all three pitch systems. In cases of no fault, the damping factors are assumed equal. However, in case of a fault in a pitch system, the parameters might be different from one pitch system to another. In order to model the hydraulic power drop and increase of air content, the parameters in the transfer function are changed during these faults. Notice here that the hydraulic pressure drop is assumed to be abrupt, whereas the air content increases slowly. The two transfer function parameters for the pressure drop case are denoted $\omega_{\mathrm{n}2}$ and ζ_2, and the two parameters for the increased air content model are denoted $\omega_{\mathrm{n}3}$ and ζ_3.

The change in the sensor gain factor induces a change in the closed-loop pitch actuator as well as a change in the measured position. Since the closed-loop pitch actuator is modeled as a linear system, the fault-induced error on the pitch position is moved from the measurement to the reference to the pitch actuator. The controller is fed by the mean value of the readings of the two sensors. Hence, this sensor fault is modeled as a change in the pitch references, meaning that a sensor fault resulting in changed mean value should also change the pitch reference accordingly

$$\beta_{\mathrm{r,f},i}[n] = \beta_{\mathrm{r},i}[n] - \frac{\Delta\beta_{i,\mathrm{m}1}[n] + \Delta\beta_{i,\mathrm{m}2}[n]}{2} \tag{7}$$

where $i \in \{1, 2, 3\}$, and $\beta_{\mathrm{r,f},i}[n]$ is the new pitch reference in which the sensor fault is contained.

C. Drive Train Model

In this benchmark model, the drive train is modeled by a two-mass model. The purpose of the drive train is to transfer torque from the rotor to the generator. It includes a gear box that increases the rotational speed from the low-speed rotor side to the high-speed generator side.

A two-mass drive train model can be represented by

$$J_{\mathrm{r}}\dot{\omega}_{\mathrm{r}}(t) = \tau_{\mathrm{r}}(t) - K_{\mathrm{dt}}\theta_{\Delta}(t) - (B_{\mathrm{dt}} + B_{\mathrm{r}})\omega_{\mathrm{r}}(t) + \frac{B_{\mathrm{dt}}}{N_{\mathrm{g}}}\omega_g(t) \tag{8}$$

$$J_{\mathrm{g}}\dot{\omega}_{\mathrm{g}}(t) = \frac{\eta_{\mathrm{dt}}K_{\mathrm{dt}}}{N_{\mathrm{g}}}\theta_{\Delta}(t) + \frac{\eta_{\mathrm{dt}}B_{\mathrm{dt}}}{N_{\mathrm{g}}}\omega_{\mathrm{r}}(t) - \left(\frac{\eta_{\mathrm{dt}}B_{dt}}{N_{\mathrm{g}}^2} + B_{\mathrm{g}}\right)\omega_{\mathrm{g}}(t) - \tau_{\mathrm{g}}(t) \tag{9}$$

$$\dot{\theta}_{\Delta}(t) = \omega_{\mathrm{r}}(t) - \frac{1}{N_{\mathrm{g}}}\omega_{\mathrm{g}}(t) \tag{10}$$

where J_{r} is the moment of inertia of the low-speed shaft, K_{dt} is the torsion stiffness of the drive train, B_{dt} is the torsion damping coefficient of the drive train, B_{g} is the viscous friction of the high-speed shaft, N_{g} is the gear ratio, J_{g} is the moment of inertia of the high-speed shaft, η_{dt} is the efficiency of the drive train, and $\theta_{\Delta}(t)$ is the torsion angle of the drive train. The fault in terms of a lower drive train efficiency is modeled by substituting another parameter, denoted $\eta_{\mathrm{dt}2}$, for η_{dt}.

D. Generator and Converter Model

The electrical system in the wind turbine and the electrical system controllers are much faster than the frequency range used in the benchmark model. On a system level of the wind turbine, the generator and converter dynamics can be modeled by a first-order transfer function

$$\frac{\tau_{\mathrm{g}}(s)}{\tau_{\mathrm{g,r}}(s)} = \frac{\alpha_{\mathrm{gc}}}{s + \alpha_{\mathrm{gc}}}$$

where α_{gc} is the generator and converter model parameter.

The power produced by the generator is given by

$$P_{\mathrm{g}}(t) = \eta_{\mathrm{g}}\omega_{\mathrm{g}}(t)\tau_{\mathrm{g}}(t)$$

where η_{g} is the efficiency of the generator.

E. Controller

The wind turbine controller in this simulation model works in two regions as previously presented. Zone 2 is denoted the power optimization and zone 3 is denoted power reference following. In the following text, zones 2 and 3, respectively, correspond to control modes 1 and 2.

In this benchmark model, a simple control scheme is used because the focus is on the fault detection and accommodation of the wind turbine. The state-of-the-art industrial controller contains typically a larger number of control modes, which provides a smoother transition between power optimization in zone 2 and constant power generation in zone 3. Another typical control feature, which is not included in the benchmark controller, is a drive train damper that is designed to attenuated drive train oscillations. Inclusion of these features in the benchmark model controller would have made it more complicated, and, on the other, lowered different transient behaviors and oscillations, which would have made the fault detection and isolation problem easier; consequently, the simple control design has been used in the benchmark model.

The controller is implemented in discrete time, with a sample frequency at 100 Hz. Subsequently, all time-dependent variables in the controller are denoted as discrete-time variables.

The controller starts in mode 1.

The control mode switches from mode 1 to 2 if

$$P_{\mathrm{g}}[n] \geq P_{\mathrm{r}}[n] \ \vee \omega_{\mathrm{g}}[n] \geq \omega_{\mathrm{nom}}$$

where ω_{nom} is the nominal generator speed. The control mode switches from mode 2 to mode 1 if

$$\omega_{\mathrm{g}}[n] < \omega_{\mathrm{nom}} - \omega_{\Delta}$$

where ω_Δ is a small offset subtracted from the nominal generator speed to introduce some hysteresis in the switching scheme, thereby avoiding that the control modes are switching all the time.

In both control modes, the controllers impose the generator torque reference and the pitch reference $\tau_{g,r}[n]$ and $\beta_r[n]$, respectively. Notice that all three pitch systems receive the same reference in this benchmark model. The control laws issuing these control signals in the two control modes are described in the following.

The fault-tolerant control scheme will depend on the nominal control scheme; much research has been conducted in many-input many-output control design for wind turbines. In this benchmark model, the commonly used industrial control scheme is used.

1) Control Mode 1: The optimal value of λ is denoted λ_{opt} and is found as the optimum point in the power coefficient (C_p) mapping of the wind turbine. The power coefficient mapping characterizes the efficiency of the energy transfer from wind energy to mechanical energy and it depend on λ and β. This optimal value is achieved by setting the pitch reference to zero ($\beta_r[n] = 0$) and the reference torque to the converter $\tau_{g,r}$ as follows:

$$\tau_{g,r}[n] = K_{opt} \cdot \left(\frac{\omega_g[n]}{N_g}\right)^2 \tag{11}$$

where

$$K_{opt} = \frac{1}{2}\rho A R^3 \frac{C_{p_{max}}}{\lambda_{opt}^3} \tag{12}$$

with ρ the air density, A the area swept by the turbine blades, and $C_{P_{max}}$ the maximum value of the power coefficient.

2) Control Mode 2: In this mode, the major control actions are handled by the pitch system using a PI controller trying to keep $\omega_g[n]$ at ω_{nom}

$$\beta_r[n] = \beta_r[n-1] + k_p e[n] + (k_i \cdot T_s - k_p)e[n-1]$$

where $e[n] = \omega_g[n] - \omega_{nom}$. In this case, the converter reference is used to suppress fast disturbances by

$$\tau_{g,r}[n] = \frac{P_r[n]}{\eta_{gc} \cdot \omega_g[n]}.$$

F. Sensors

Each sensor is modeled by the sum of the actual variable value and a stochastic noise. The mean value and the variance of the noise are denoted as follows for the various measurements:

m_w, σ_w(wind speed - v_w);
$m_{\omega_r}, \sigma_{\omega_r}$ (rotor speed - ω_r);
$m_{\omega_g}, \sigma_{\omega_g}$ (generator speed - ω_g);
$m_{\tau_g}, \sigma_{\tau_g}$ (generator torque - τ_g);
m_{P_g}, σ_{P_g} (generator power - P_g);
m_β, σ_β (pitch angle - β).

Notice that for rotor speed, generator speed, pitch angles, and multiple sensors of the same kind are contained in the wind turbine, and in this simulation model all sensors of the same kind have the same stochastic parameters.

TABLE II
WIND MODEL PARAMETERS USED IN THE BENCHMARK MODEL

α	H	r_0
0.1	81 m	1.5 m

TABLE III
BLADE AND PITCH MODEL PARAMETERS USED IN THE BENCHMARK MODEL

R	ρ	ζ	ω_n
57.5 m	$1.225\frac{kg}{m^3}$	0.6	$11.11\frac{rad}{s}$
ζ_2	ω_{n2}	ζ_3	ω_{n3}
0.45	$5.73\frac{rad}{s}$	0.9	$3.42\ \frac{rad}{s}$

TABLE IV
DRIVE TRAIN MODEL PARAMETERS USED IN THE BENCHMARK MODEL

B_{dt}	B_r	B_g	N_g
$775.49\ \frac{Nms}{rad}$	$7.11\ \frac{Nms}{rad}$	$45.6\ \frac{Nms}{rad}$	95
K_{dt}	η_{dt}	η_{dt2}	J_g
$2.7\ \cdot 10^9\ \frac{Nm}{rad}$	0.97	0.92	$390\ kg \cdot m^2$
J_r			
$55 \cdot 10^6\ kg \cdot m^2$			

G. Model Parameters

The parameters used in the benchmark model are listed in the following tables. The wind model parameters can be found in Table II, and the blade and pitch model parameters can be seen in Table III. Table IV shows the drive train model parameters. The generator and converter model parameters can be seen in Table V. The used controller parameters can be found in Table VI. The parameters used in the sensor models are shown in Table VII.

V. TEST SIGNALS DEFINITION

In the test signal definition described in [7], the defined faults are present at a predefined time. This paper introduces six additional test signal sets; they are formed by time-shifting the occurrence of the faults defined in the original benchmark model. This is done to check that the proposed FDI and FTC schemes are robust toward different points of operation for the faults in question. In this benchmark model setup, a predefined wind speed sequence is used. This wind sequence consists of real measured wind data from a wind park. This wind speed sequence can be seen in Fig. 6.

In the listing of the possible faults, a subset is chosen for the benchmark test sequence.

The test includes five sensors faults, three actuator faults, and one system fault. In the initial test set (test set 1), faults are presented in the same order as in Table I. The time shift for the different test sets can be seen below.

1) Test set 2: +100 s for all faults.
2) Test set 3: −100 s for all faults.

TABLE V
GENERATOR AND CONVERTER MODEL PARAMETERS USED IN THE BENCHMARK MODEL

α_{gc}	η_{gc}
50 $\frac{rad}{s}$	0.98

TABLE VI
CONTROLLER PARAMETERS USED IN THE BENCHMARK MODEL

K_{opt}	K_i	K_p	ω_{nom}	ω_Δ	P_r
1.2171	1	4	162 $\frac{rad}{s}$	15 $\frac{rad}{s}$	$4.8 \cdot 10^6$ W

TABLE VII
SENSORS MODEL PARAMETERS USED IN THE BENCHMARK MODEL

m_w	σ_w	m_{ω_r}	σ_{ω_r}	m_{ω_g}	σ_{ω_g}
1.5 $\frac{m}{s}$	0.5 $\frac{m}{s}$	0 $\frac{rad}{s}$	0.025 $\frac{rad}{s}$	0 $\frac{rad}{s}$	0.05 $\frac{rad}{s}$
m_{τ_g}	σ_{τ_g}	m_{P_g}	σ_{P_g}	m_β	σ_β
0 Nm	90 Nm	0 W	$1 \cdot 10^3$ W	0°	0.2°

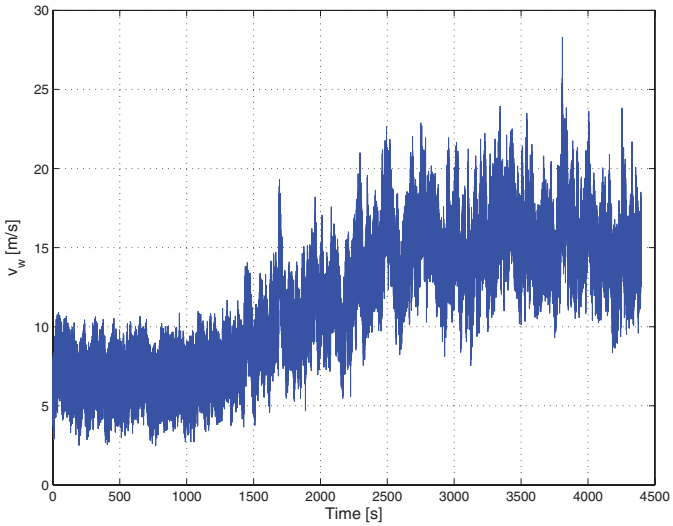

Fig. 6. Illustration of the wind speed sequence used in the benchmark model. It can be seen that the wind speed covers the range 5–20 m/s, with a few spikes at 25 m/s, which is a good coverage of normal operational for a wind turbine.

3) Test set 4: −200 s for all faults.
4) Test set 5: −300 s for all faults.
5) Test set 6: −400 s for all faults.
6) Test set 7: −500 s for all faults.

It should be noticed that the schemes described in this paper are only designed based on test series 1.

In the following, test set 1 is defined and the different measurement signals are plotted as well. The fault parameters are chosen such that they result in faults that are of such a size that they influence the wind turbine performance and they are detectable and isolatable. On the other hand, they are chosen small enough so that they should be a challenge to detect and isolate. The actual values were found by trial and error on the benchmark model before it was originally published. One fault parameter has been changed in the original model: the offset on τ_g. The orginal value was 2000 Nm, which is now changed to 100 Nm. The change was made in order to make detection and isolation of this fault more challenging. It should be noticed that the contributors of the schemes evaluated in this paper were aware of this parameter change before they finalized their designs.

The fault occurrence scenario is the following.

1) Fault 1: fault type A1, a fixed value on $\beta_{1,m1}$ equal to 5° in the time period from 2000 to 2100 s.
2) Fault 2: fault type A2, a gain factor on $\beta_{2,m2}$ equal to 1.2 in the time period from 2300 to 2400 s.
3) Fault 3: fault type A1, a fixed value on $\beta_{3,m1}$ equal to 10° in the time period from 2600 to 2700 s.
4) Fault 4: fault type A3, a fixed value on $\omega_{r,m1}$ equal to 1.4 rad/s in the time period from 1500 to 1600 s.
5) Fault 5: fault types A4 and A6, gain factors on $\omega_{r,m2}$ and $\omega_{g,m1}$, respectively, equal to 1.1 and 0.9 in the time period from 1000 to 1100 s.
6) Fault 6: fault type B3, change in the dynamics due to hydraulic pressure drop of the pitch actuator 2; the fault is assumed to be abrupt and it is present in the time period from 2900 to 3000 s.
7) Fault 7: fault type B4, change in the dynamics due to increased air content in the oil on pitch actuator 3. The fault is slowly introduced during 30 s with a constant rate; afterward the fault is active during 40 s, and again decreases during 30 s. The fault begins at 3500 s and ends at 3600 s.
8) Fault 8: fault type B2, an offset on τ_g of the value 100 Nm, the fault is active from 3800 to 3900 s.
9) Fault 9: fault type C1, a change in the friction in the drive train active from 4100 to 4300 s.

These faults must be detected and handled according to the previously stated requirements. In order to validate the false positive rate of the detection scheme, a set of data simulated on an advanced model of the wind turbine is provided for a fault-free run on the same wind speed sequence.

Plots of some of the relevant states and measurements during this sequence of wind input and defined faults are presented in Figs. 7–14. The power, rotor speed, rotor speed measurements, generator speed measurement, and pitch angle measurements can be seen.

The benchmark model package contains a wind speed sequence, which is a Simulink model with a parameter file. The package can be obtained at [35].

A. Additional Test Scenarios

It is relevant to test fault detection, isolation, and accommodation with multiple occurring faults. The most challenging situation typically occurs when faults affect interacting subparts of the wind turbine. An example of such a scenario is suggested below.

1) Fault A: fault type A2, a gain factor on $\beta_{2,m2}$ equal to 1.2 in the time period from 2300 to 2600 s.
2) Fault B: fault type B3, change in the dynamics due to hydraulic pressure drop of the pitch actuator 2; the fault is assumed to be abrupt and it is present in the time period from 2305 to 2600 s.

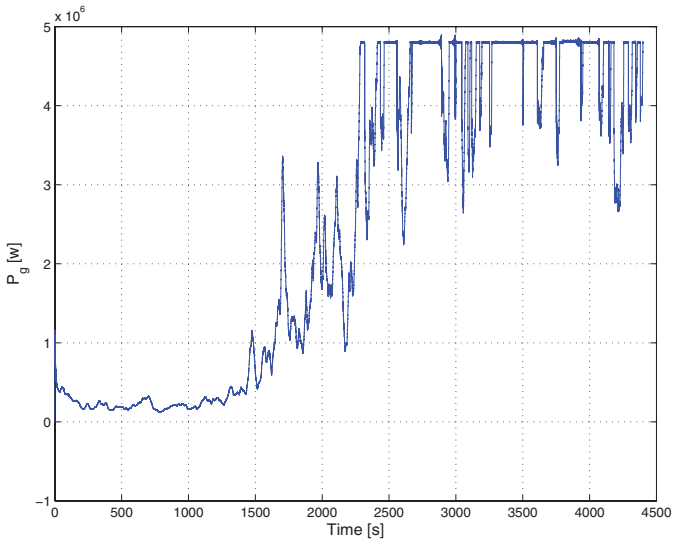

Fig. 7. Wind turbine active power as output of the simulation with the defined faults present. It can be seen that the different faults decrease the power generation. This is easy to see in the region of full power from approximately 1900 s to the end; the drops in power below the full power level are due to faults in the wind turbine.

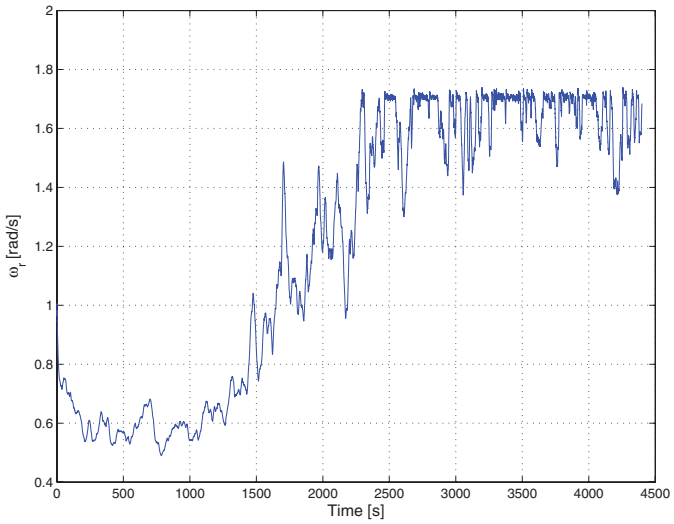

Fig. 8. Rotor speed value as output of the simulation with the defined faults present. The rotor speed is influenced by all the faults as with the generated power.

3) Fault C: fault type A1, a fixed value on $\beta_{1,\mathrm{m1}}$ equal to 5° in the time period from 2600 to 3000 s.
4) Fault D: fault type B4, change in the dynamics due to increased air content in the oil on pitch actuator 3. The fault is slowly introduced during 30 s with a constant rate; afterward the fault is active during 40 s, and again decreases during 30 s. The fault begins at 2605 s and ends at 3000 s.
5) Fault E: fault type B2, an offset on τ_{g} of the value 100 Nm, the fault is active from 3800 to 4400 s.
6) Fault F: fault types A4 and A6, gain factors on $\omega_{\mathrm{r,m2}}$ and $\omega_{\mathrm{g,m1}}$, respectively, equal to 1.1 and 0.9 in the time period from 3805 to 4400 s.

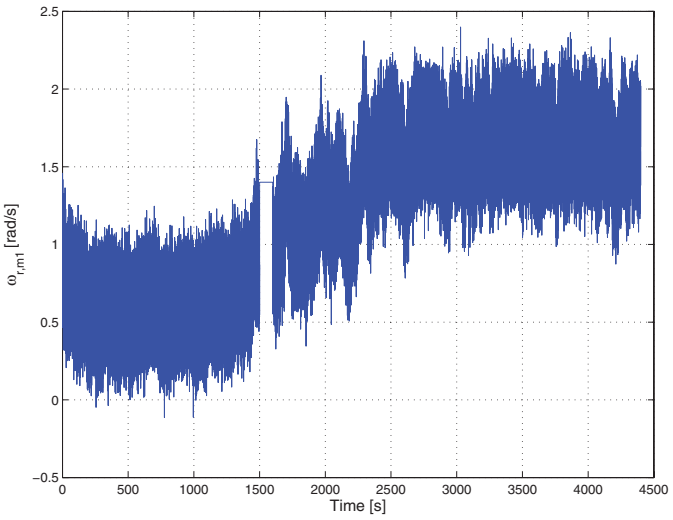

Fig. 9. Measured rotor speed value from Sensor 1 as output of the simulation with the defined faults present. It can be seen that this sensor signal is fixed in the time interval 1500–1600 s.

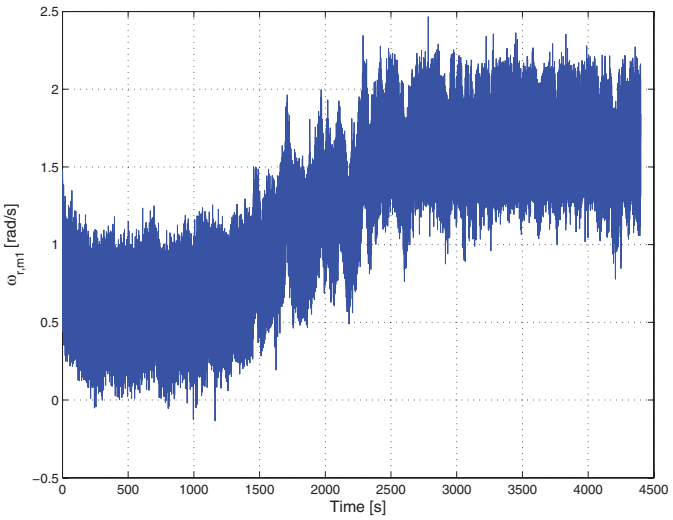

Fig. 10. Measured rotor speed value from Sensor 2 as output of the simulation with the defined faults present. This sensor has a fault given as a gain factor of 1.1 in the time interval 1000–1100 s.

VI. Description of FDI Solutions

In this section, five solutions to the problems given in the wind turbine benchmark model are shortly introduced.

A. Gaussian Kernel Support Vector Machine Solution (GKSV)

This scheme is based on a support vector machine built on a Gaussian kernel, and is presented in [9]. In this design, a vector x of features is defined for each fault, which contains relevant measurements, filtered measurements, or combinations of these. Depending of the fault type, two–four features are used.

Residuals for all of the defined faults are obtained by projecting the feature vectors on the kernel of the support vector machine. Among a number of tested kernels, a Gaussian kernel with different variance values was found to be the best one for all faults.

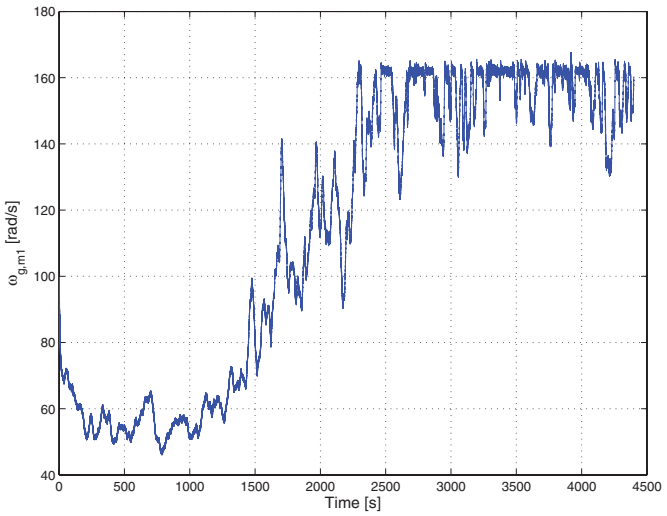

Fig. 11. Measured generator speed value from Sensor 1 as output of the simulation with the defined faults present. This sensor has a fault in the time period from 1000 to 1100 s, in which the sensor has a gain factor of 0.9.

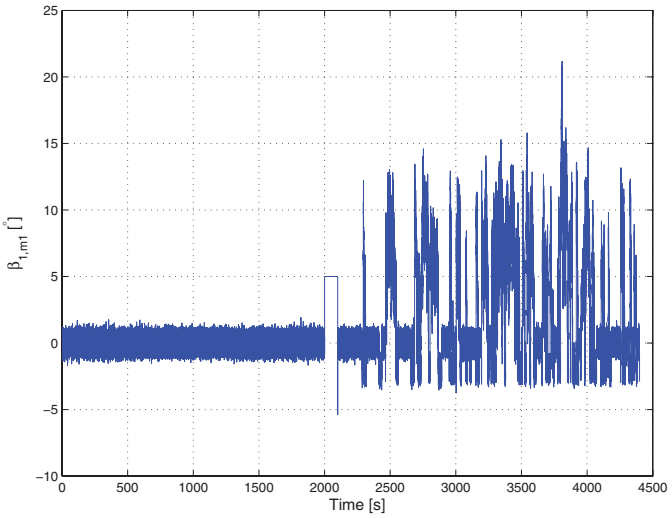

Fig. 12. Measured pitch angle of Blade 1 from Sensor 1 as output of the simulation with the defined faults present. The fault in this sensor results in a fixed value in the time interval from 2000 to 2100 s.

Data with and without faults were used for learning the model for FDI of the specific faults, and, based on this the vectors, kernel (structure and parameters) were found.

B. Estimation-Based Solution (EB)

The general outline of this scheme is that a fault detection estimator is designed to determine the presence of a fault, and an additional bank of N isolation estimators is designed to isolate the faults, where N is the number of faults considered. As described in [12], it is a preliminary and simplified implementation of the general method given in [39] and [40]. Specifically, the method in [12] is designed on the basis of a linear system model and without the use of an adaptive threshold. The estimators used for FDI are designed on the basis of the provided models including model parameters. Each isolation estimator is designed on the basis of a particular fault scenario under consideration.

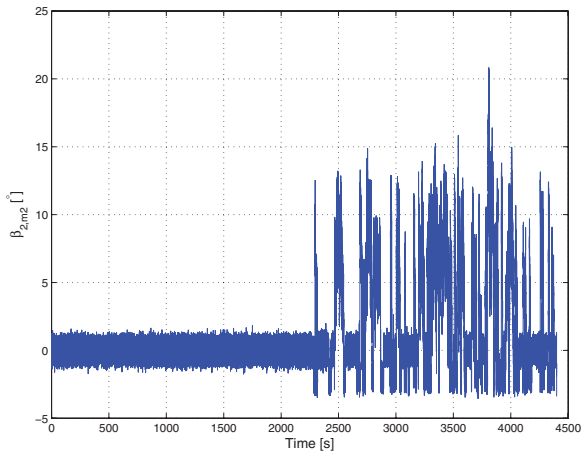

Fig. 13. Measured pitch angle of Blade 2 from Sensor 2 as output of the simulation with the defined faults present. In the time interval from 2300 to 2400 s, a gain factor of 1.2 is introduced.

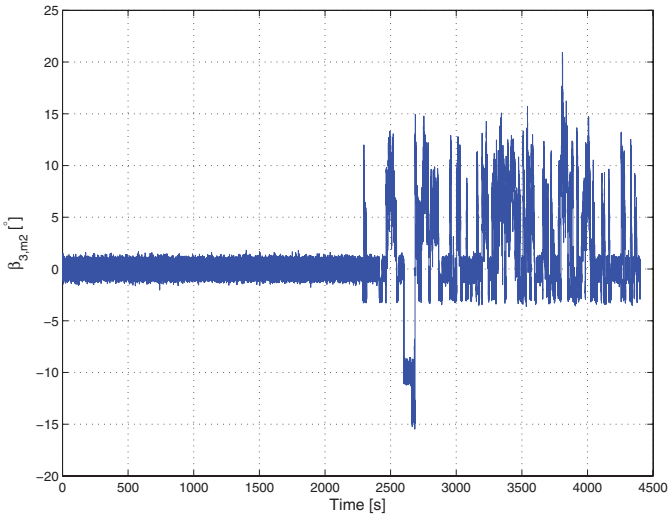

Fig. 14. Measured pitch angle of Blade 3 from Sensor 2 as output of the simulation with fault scenarios. The output of this sensor is fixed in the interval from 2600 to 2700 s.

C. Up-Down Counter Solution (UDC)

Up-down counters are used in this solution for decision of FDI based on residuals for each of the faults. The details of the solutions can be found in [10]. The FDI residuals are based on residuals obtained by physical redundancy, parity equations, Kalman filters, and other filters.

There are two major differences between the used up-down counters and straightforward thresholding methods. The first is that the decision to declare a fault involves discrete-time dynamics and is not simply a function of the current value of the residual. The second is that a penalty on the residual exceeding the threshold is introduced in this scheme.

D. Combined Observer and Kalman Filter Solution (COK)

This solution uses a diagnostic-observer-based residual generator for residual generation for the faults in the drive train, in which the wind speed also is considered as a disturbance. Details on this scheme can be found in [8].

TABLE VIII
RESULTS OF EVALUATION FAULTS 1–3

Fault	GKSV	EB	UDC	COK	GFM
1	$\overline{T}_{\mathrm{d}} = 0.02$ [s], $T_{\underline{\mathrm{d}}} = 0.02$ [s], $T_{\overline{\mathrm{d}}} = 0.02$ [s], $F_{\mathrm{D}} = 0$, $F_{\underline{\mathrm{d}}} = 0$, $F_{\overline{\mathrm{d}}} = 0$	$\overline{T}_{\mathrm{d}} = 0.02$ [s], $T_{\underline{\mathrm{d}}} = 0.01$ [s], $T_{\overline{\mathrm{d}}} = 0.02$ [s], $F_{\mathrm{D}} = 0$, $F_{\underline{\mathrm{d}}} = 0$, $F_{\overline{\mathrm{d}}} = 0$, $MD_{\mathrm{D}} = 3\%$, $MD_{\min} = 0\%$, $MD_{\max} = 20\%$	$\overline{T}_{d} = 0.03$ [s], $T_{\underline{\mathrm{d}}} = 0.02$ [s], $T_{\overline{\mathrm{d}}} = 0.03$ [s], $F_{\mathrm{D}} = 0$, $F_{\underline{\mathrm{d}}} = 0$, $F_{\overline{\mathrm{d}}} = 0$	$\overline{T}_{d} = 10.32$ [s], $T_{\underline{\mathrm{d}}} = 10.23$ [s], $T_{\overline{\mathrm{d}}} = 10.33$ [s], $F_{\mathrm{D}} = 0.89$, $F_{\underline{\mathrm{d}}} = 0$, $F_{\overline{\mathrm{d}}} = 1$	$\overline{T}_{d} = 0.04$ [s], $T_{\underline{\mathrm{d}}} = 0.03$ [s], $T_{\overline{\mathrm{d}}} = 0.04$ [s], $F_{\mathrm{D}} = 0$, $F_{\underline{\mathrm{d}}} = 0$, $F_{\overline{\mathrm{d}}} = 0$
2	$\overline{T}_{d} = 47.24$ [s], $T_{\underline{\mathrm{d}}} = 3.23$ [s], $T_{\overline{\mathrm{d}}} = 95.09$ [s], $F_{\mathrm{D}} = 0$, $F_{\underline{\mathrm{d}}} = 0$, $F_{\overline{\mathrm{d}}} = 0$, $MD_{\mathrm{D}} = 56\%$, $MD_{\min} = 0\%$, $MD_{\max} = 100\%$	$\overline{T}_{d} = 44.65$ [s], $T_{\underline{\mathrm{d}}} = 0.63$ [s], $T_{\overline{\mathrm{d}}} = 95.82$ [s], $F_{\mathrm{D}} = 22$, $F_{\underline{\mathrm{d}}} = 16$, $F_{\overline{\mathrm{d}}} = 28$, $MD_{\mathrm{D}} = 56\%$, $MD_{\min} = 0\%$, $MD_{\max} = 100\%$	$\overline{T}_{d} = 69.12$ [s], $T_{\underline{\mathrm{d}}} = 7.60$ [s], $T_{\overline{\mathrm{d}}} = 95.72$ [s], $F_{\mathrm{D}} = 0$, $F_{\underline{\mathrm{d}}} = 0$, $F_{\overline{\mathrm{d}}} = 0$, $MD_{\mathrm{D}} = 67\%$, $MD_{\min} = 0\%$, $MD_{\max} = 100\%$	$\overline{T}_{d} = 19.24$ [s], $T_{\underline{\mathrm{d}}} = 3.43$ [s], $T_{\overline{\mathrm{d}}} = 49.93$ [s], $F_{\mathrm{D}} = 0.97$, $F_{\underline{\mathrm{d}}} = 0$, $F_{\overline{\mathrm{d}}} = 5$	$\overline{T}_{d} = 13.70$ [s], $T_{\underline{\mathrm{d}}} = 0.38$ [s], $T_{\overline{\mathrm{d}}} = 25.32$ [s], $F_{\mathrm{D}} = 3.08$, $F_{\underline{\mathrm{d}}} = 1$, $F_{\overline{\mathrm{d}}} = 18$
3	$\overline{T}_{d} = 0.02$ [s], $T_{\underline{\mathrm{d}}} = 0.02$ [s], $T_{\overline{\mathrm{d}}} = 0.02$ [s], $F_{\mathrm{D}} = 0$, $F_{\underline{\mathrm{d}}} = 0$, $F_{\overline{\mathrm{d}}} = 0$	$\overline{T}_{d} = 0.54$ [s], $T_{\underline{\mathrm{d}}} = 0.51$ [s], $T_{\overline{\mathrm{d}}} = 0.76$ [s], $F_{\mathrm{D}} = 4$, $F_{\underline{\mathrm{d}}} = 1$, $F_{\overline{\mathrm{d}}} = 11$, $MD_{\mathrm{D}} = 3\%$, $MD_{\min} = 0\%$, $MD_{\max} = 20\%$	$\overline{T}_{d} = 0.04$ [s], $T_{\underline{\mathrm{d}}} = 0.03$ [s], $T_{\overline{\mathrm{d}}} = 0.10$ [s], $F_{\mathrm{D}} = 0$, $F_{\underline{\mathrm{d}}} = 0$, $F_{\overline{\mathrm{d}}} = 0$, $MD_{\mathrm{D}} = 3\%$, $MD_{\min} = 0\%$, $MD_{\max} = 20\%$	$\overline{T}_{d} = 10.35$ [s], $T_{\underline{\mathrm{d}}} = 1.54$ [s], $T_{\overline{\mathrm{d}}} = 10.61$ [s], $F_{\mathrm{D}} = 1.42$, $F_{\underline{\mathrm{d}}} = 1$, $F_{\overline{\mathrm{d}}} = 4$	$\overline{T}_{d} = 0.05$ [s], $T_{\underline{\mathrm{d}}} = 0.03$ [s], $T_{\overline{\mathrm{d}}} = 0.06$ [s], $F_{\mathrm{D}} = 1.61$, $F_{\underline{\mathrm{d}}} = 1$, $F_{\overline{\mathrm{d}}} = 5$

TABLE IX
RESULTS OF EVALUATION FAULTS 4–6

Fault	GKSV	EB	UDC	COK	GFM
4	$\overline{T}_{d} = 0.11$ [s], $T_{\underline{\mathrm{d}}} = 0.09$ [s], $T_{\overline{\mathrm{d}}} = 0.18$ [s], $F_{\mathrm{D}} = 0$, $F_{\underline{\mathrm{d}}} = 0$, $F_{\overline{\mathrm{d}}} = 0$	$\overline{T}_{d} = 0.33$ [s], $T_{\underline{\mathrm{d}}} = 0.27$ [s], $T_{\overline{\mathrm{d}}} = 0.44$ [s], $F_{\mathrm{D}} = 0$, $F_{\underline{\mathrm{d}}} = 0$, $F_{\overline{\mathrm{d}}} = 0$	$\overline{T}_{d} = 0.02$ [s], $T_{\underline{\mathrm{d}}} = 0.02$ [s], $T_{\overline{\mathrm{d}}} = 0.02$ [s], $F_{\mathrm{D}} = 1$, $F_{\underline{\mathrm{d}}} = 1$, $F_{\overline{\mathrm{d}}} = 8$	$\overline{T}_{d} = 0.18$ [s], $T_{\underline{\mathrm{d}}} = 0.03$ [s], $T_{\overline{\mathrm{d}}} = 0.46$ [s], $F_{\mathrm{D}} = 2.31$, $F_{\underline{\mathrm{d}}} = 0$, $F_{\overline{\mathrm{d}}} = 5$	$\overline{T}_{d} = 0.10$ [s], $T_{\underline{\mathrm{d}}} = 0.03$ [s], $T_{\overline{\mathrm{d}}} = 0.34$ [s], $F_{\mathrm{D}} = 3.36$, $F_{\underline{\mathrm{d}}} = 1$, $F_{\overline{\mathrm{d}}} = 18$
5	$\overline{T}_{d} = 25.90$ [s], $T_{\underline{\mathrm{d}}} = 1.24$ [s], $T_{\overline{\mathrm{d}}} = 87.49$ [s], $F_{\mathrm{D}} = 0$, $F_{\underline{\mathrm{d}}} = 0$, $F_{\overline{\mathrm{d}}} = 0$, $(\overline{\mathrm{MD}})_{\mathrm{D}} = 3\%$, $MD_{\min} = 0\%$, $MD_{\max} = 20\%$	$\overline{T}_{d} = 0.01$ [s], $T_{\underline{\mathrm{d}}} = 0.01$ [s], $T_{\overline{\mathrm{d}}} = 0.01$ [s], $F_{\mathrm{D}} = 117$, $F_{\underline{\mathrm{d}}} = 95$, $F_{\overline{\mathrm{d}}} = 142$	$\overline{T}_{d} = 2.96$ [s], $T_{\underline{\mathrm{d}}} = 0.38$ [s], $T_{\overline{\mathrm{d}}} = 21.08$ [s], $F_{\mathrm{D}} = 0.75$, $F_{\underline{\mathrm{d}}} = 0$, $F_{\overline{\mathrm{d}}} = 3$	$\overline{T}_{d} = 31.32$ [s], $T_{\underline{\mathrm{d}}} = 1.54$ [s], $T_{\overline{\mathrm{d}}} = 91.13$ [s], $F_{\mathrm{D}} = 0.26$, $F_{\underline{\mathrm{d}}} = 0$, $F_{\overline{\mathrm{d}}} = 2$, $(\overline{\mathrm{MD}})_{\mathrm{D}} = 14\%$, $MD_{\min} = 0\%$, $MD_{\max} = 40\%$	$\overline{T}_{d} = 9.49$ [s], $T_{\underline{\mathrm{d}}} = 0.56$ [s], $T_{\overline{\mathrm{d}}} = 17.18$ [s], $F_{\mathrm{d}} = 2.42$, $F_{\underline{\mathrm{d}}} = 1$, $F_{\overline{\mathrm{d}}} = 18$
6	$(\overline{\mathrm{MD}})_{\mathrm{D}} = 100\%$, $MD_{\min} = 100\%$, $MD_{\max} = 100\%$	$\overline{T}_{d} = 11.31$ [s], $T_{\underline{\mathrm{d}}} = 0.06$ [s], $T_{\overline{\mathrm{d}}} = 55.27$ [s], $F_{\mathrm{D}} = 2$, $F_{\underline{\mathrm{d}}} = 0$, $F_{\overline{\mathrm{d}}} = 20$	$\overline{T}_{d} = 11.81$ [s], $T_{\underline{\mathrm{d}}} = 0.53$ [s], $T_{\overline{\mathrm{d}}} = 55.72$ [s], $F_{\mathrm{D}} = 22$, $F_{\underline{\mathrm{d}}} = 15$, $F_{\overline{\mathrm{d}}} = 25$	$\overline{T}_{d} = 23.80$ [s], $T_{\underline{\mathrm{d}}} = 0.33$ [s], $T_{\overline{\mathrm{d}}} = 64.95$ [s], $F_{\mathrm{D}} = 0.03$, $F_{\underline{\mathrm{d}}} = 0$, $F_{\overline{\mathrm{d}}} = 3$	$\overline{T}_{d} = 15.52$ [s], $T_{\underline{\mathrm{d}}} = 0.02$ [s], $T_{\overline{\mathrm{d}}} = 61.13$ [s], $F_{\mathrm{D}} = 3.67$, $F_{\underline{\mathrm{d}}} = 1$, $F_{\overline{\mathrm{d}}} = 37$

This diagnostic observer is designed to decouple the disturbance and simultaneously achieve the optimal residual generation with respect to process and sensor noise models. A Kalman-filter-based scheme is designed for two of the subsystems. Generalized likelihood ratio test and cumulative variance index are used for fault decision based on the statistical properties of the residual signals. For the fault isolation purpose, a bank of residual generators based on dual sensor redundancy is designed. The residual bank is used to isolate the sensor faults, and system faults are isolated by a decision table. A compensation strategy for the closed-loop pitch system is used for the FDI system of the pitch sensor faults.

E. General Fault Model Solution (GFM)

This solution is an automatic generated solution for FDI; the details can be seen in [11]. Three main steps in the design of this proposed method are: 1) a large set of potential residual generators are generated; 2) the most suitable residual generators are selected and then constructed by use of the algorithms presented in [41] (the selection is done by means of a greedy selection algorithm); and 3) the diagnostic tests for the selected set of residual generators are designed. A comparison between the estimated probability distributions of residuals is used for diagnostic tests and evaluated with faulty and no-fault data.

TABLE X
RESULTS OF EVALUATION FAULTS 7 AND 8

Fault	GKSV	EB	UDC	COK	GFM
7	$\overline{(\mathrm{MD})}_{\mathrm{D}} = 100\%$, $MD_{\min} = 100\%$, $MD_{\max} = 100\%$	$\overline{T}_d = 26.07$ [s], $T_{\underline{\mathrm{d}}} = 3.33$ [s], $T_{\overline{\mathrm{d}}} = 52.66$ [s], $\overline{F}_{\mathrm{D}} = 1.8$, $F_{\underline{\mathrm{d}}} = 1$, $F_{\overline{\mathrm{d}}} = 5$	$\overline{T}_d = 12.93$ [s], $T_{\underline{\mathrm{d}}} = 2.86$ [s], $T_{\overline{\mathrm{d}}} = 51.08$ [s], $\overline{F}_{\mathrm{D}} = 2$, $F_{\underline{\mathrm{d}}} = 1$, $F_{\overline{\mathrm{d}}} = 4$	$\overline{T}_d = 34.00$ [s], $T_{\underline{\mathrm{d}}} = 17.22$ [s], $T_{\overline{\mathrm{d}}} = 52.93$ [s], $\overline{F}_{\mathrm{D}} = 0$, $F_{\underline{\mathrm{d}}} = 0$, $F_{\overline{\mathrm{d}}} = 0$	$\overline{T}_d = 31.70$ [s], $T_{\underline{\mathrm{d}}} = 0.61$ [s], $T_{\overline{\mathrm{d}}} = 180.70$ [s], $\overline{F}_{\mathrm{D}} = 1.25$, $F_{\underline{\mathrm{d}}} = 1$, $F_{\overline{\mathrm{d}}} = 5$
8	$\overline{T}_d = 0.01$ [s], $T_{\underline{\mathrm{d}}} = 0.01$ [s], $T_{\overline{\mathrm{d}}} = 0.01$ [s], $\overline{F}_{\mathrm{D}} = 0$, $F_{\underline{\mathrm{d}}} = 0$, $F_{\overline{\mathrm{d}}} = 0$, $\overline{(\mathrm{MD})}_{\mathrm{D}} = 97\%$, $MD_{\min} = 0\%$, $MD_{\max} = 100\%$	$\overline{T}_d = 0.01$ [s], $T_{\underline{\mathrm{d}}} = 0.01$ [s], $T_{\overline{\mathrm{d}}} = 0.01$ [s], $\overline{F}_{\mathrm{D}} = 0$, $F_{\underline{\mathrm{d}}} = 0$, $F_{\overline{\mathrm{d}}} = 0$, $\overline{(\mathrm{MD})}_{\mathrm{D}} = 97\%$, $MD_{\min} = 0\%$, $MD_{\max} = 100\%$	$\overline{T}_d = 0.02$ [s], $T_{\underline{\mathrm{d}}} = 0.02$ [s], $T_{\overline{\mathrm{d}}} = 0.02$ [s], $\overline{F}_{\mathrm{D}} = 0$, $F_{\underline{\mathrm{d}}} = 0$, $F_{\overline{\mathrm{d}}} = 0$, $\overline{(\mathrm{MD})}_{\mathrm{D}} = 97\%$, $MD_{\min} = 0\%$, $MD_{\max} = 100\%$	$\overline{T}_d = 0.01$ [s], $T_{\underline{\mathrm{d}}} = 0.01$ [s], $T_{\overline{\mathrm{d}}} = 0.01$ [s], $\overline{F}_{\mathrm{D}} = 0$, $F_{\underline{\mathrm{d}}} = 0$, $F_{\overline{\mathrm{d}}} = 0$, $\overline{(\mathrm{MD})}_{\mathrm{D}} = 97\%$, $MD_{\min} = 0\%$, $MD_{\max} = 100\%$	$\overline{T}_d = 7.92$ [s], $T_{\underline{\mathrm{d}}} = 7.92$ [s], $T_{\overline{\mathrm{d}}} = 7.92$ [s], $\overline{F}_{\mathrm{D}} = 0$, $F_{\underline{\mathrm{d}}} = 0$, $F_{\overline{\mathrm{d}}} = 0$, $\overline{(\mathrm{MD})}_{\mathrm{D}} = 97\%$, $MD_{\min} = 0\%$, $MD_{\max} = 100\%$

VII. EVALUATION OF SOLUTIONS

In this section, the five solutions presented in Section VI are compared on simulations with all seven test series and for all eight faults. The mean, minimum, and maximum values of fault detection time (T_{d}), the number of false positive detections (F_{D}), and missed detections (MD) are computed for the different methods. This means that these variables are computed for a given fault taking all simulations in all test series into account.

The following notation is used: $\overline{T}_{\mathrm{d}}$ denotes the mean value of the detection time; $T_{\underline{\mathrm{d}}}$ denotes the minimum value of the detection time; $T_{\overline{\mathrm{d}}}$ denotes the maximum value of the detection time; $\overline{F}_{\mathrm{D}}$ denotes the mean value of the number of false positive detections; $F_{\underline{\mathrm{d}}}$ denotes the minimum value of the number of false positive detections; $F_{\overline{\mathrm{d}}}$ denotes the maximum value of the number of false positive detections; $\overline{\mathrm{MD}}_{\mathrm{d}}$ denotes the mean percentage of missed detection in a test series; $\mathrm{MD}_{\min}$ denotes the minimum percentage of missed detections in a test series; and $\mathrm{MD}_{\max}$ denotes the maximum percentage of missed detections in a test series. In case no information on missed detections is provided, no missed detections were present, meaning that all missed detection statistics were zero for the specific method for all test series. The results of the evaluation are shown in Table VIII for faults 1–3, in Table IX for faults 4–6, and in Table X for faults 7 and 8. None of the proposed schemes was designed for detection and isolation of fault 9, so these are not included in the tables.

In general, all schemes only detected fault 8 in test series 1, (which they are designed on). The reason for this is that a change in the occurrence time of this fault will change the ratio between the offset and the requested generator torque, and since the offset is relatively small, this will make it very difficult to detect this fault in the other test series unless the algorithms were designed for these new generator torque reference levels. This also leads to identical missed detection statistics for all schemes for fault 8. Most of the schemes did have problems detecting and isolating fault 2 for the higher test series numbers. The reason for this is that this fault is a gain factor on one of the pitch sensors and the mentioned test series include a low level of pitch values for these series since the wind speed is low. An active FDI scheme would be better for these faults, as proposed in [3].

In the following, some observations on the performance of the specific schemes are presented. Computational time has not been an evaluation criterion, since the proposed schemes have not been optimized in terms of computational time. Consequently, no comments are given on the computational times for the specific schemes.

GKSV only detects and isolates the sensor faults 1–5. Faults 1, 3, and 4 are detected within the specifications in all test series without any false positive detections. For those faults, the scheme is independent of the time location of the faults and therefore the point of operation at which the faults occurs. This scheme thus provides good robustness toward the changed point of operation of the faults. It should also be noticed here that, even though that the scheme is data driven, system knowledge have been used to select the relevant measurements for the different faults. It is also critical which data is used in the design process, e.g., whether the fault-free data cover the entire operational range, and whether it is actually fault free. In the benchmark case, the general wind speed sequence is the same in all simulations faulty or fault free. The scheme might have encountered difficulties if the test wind speed were to contain values not included in the wind speed sequence used in the design case. It is expected that this method can be applied to the actuator and system faults as well.

EB detects and isolates overall the faults fast for the original test series and slower as the fault time location, and thereby the operational point moves away from the test series 1. A large number of false positive detections are present for some faults. Clearly, the large number of false positive detections could be lowered by a different choice of design parameters. The estimator design requires knowledge of both the model as well as the used estimator technique. It would be necessary to design the estimators for the different points of operation of the faults in order to ensure a constant performance of the scheme.

UDC detects and isolates almost all faults in all test series. Most of the faults were well detected and isolated relatively fast, but with some false positive detection. The tests also showed that this scheme is relatively robust toward

the operational point at which the faults occur. Knowledge of the model was used to find the best and simplest suited residual generators for the different faults. The advantage of this is that the detection and isolation scheme is dedicated to specific faults, but, on the other hand, it also requires time and knowledge in the design process to find the best solution. It is expected that the UDC scheme could be returned to lower the number of false positive detections, and this decision rule provides a good balancing between fast detections and avoidance of false positive detections.

COK detects and isolates most of the faults in all test series. This is, however, done slowly and for most of the faults slower than required. The tests did also show a few false positive detections for most of faults. Again, it is a scheme based on a model that requires knowledge of the system, model, used observers, and Kalman filters. It would probably improve the performance of this scheme if it were returned to provide faster detection even though it would increase the number of false positive detections slightly.

GFM detects and isolates all faults (except fault 8) in all test series slowly and with some false positive detections. This scheme performs better than the other schemes, as the operational point of the faults are moving further away from the operational points of test series 1. This indicates a scheme robust toward the point of operation of the faults. The major advantage of this scheme is that it requires a very low level of system knowledge and a simple system model. The detection and isolation scheme is automatically generated based on all possible residuals. It provides a working solution, which, however, is not as good as the other tested solutions when faults occurs close to the values in test series 1, in terms of detection time, etc., The fact that it is performing better as the point of operation of the faults moves away from design point indicates that the generic nature of the design process introduces some robustness in the design, simply because it is not optimally designed.

VIII. Conclusion

In this paper, a benchmark model for testing fault detection and fault accommodation schemes in wind turbines was presented. The model simulates the actuator, sensor, and system faults in the pitch actuators, drive train, and converter system. Various kinds of faults were included in this test bench model. Seven different test series were presented with different time locations of the faults, which corresponded to different operating points at which the faults occurred. Five different FDI schemes designed on one of these test series were evaluated on all seven series.

References

[1] X. Wei, M. Verhaegen, and T. van den Engelen, "Sensor fault diagnosis of wind turbines for fault tolerant," in *Proc. 17th World Congr. Int. Fed. Autom. Control*, Jul. 2008, pp. 3222–3227.

[2] P. F. Odgaard, J. Stoustrup, R. Nielsen, and C. Damgaard, "Observer based detection of sensor faults in wind turbines," in *Proc. Eur. Wind Energy Conf.*, Mar. 2009, pp. 1–6.

[3] C. Sloth, T. Esbensen, and J. Stoustrup, "Active and passive fault-tolerant LPV control of wind turbines," in *Proc. Amer. Control Conf.*, Jun. 2010, pp. 4640–4646.

[4] K. Rothenhagen and F. W. Fuchs, "Current sensor fault detection and reconfiguration for a doubly fed induction generator," in *Proc. IEEE Power Electron. Specialists Conf.*, Jun. 2007, pp. 2732–2738.

[5] K. Rothenhagen, S. Thomsen, and F. W. Fuchs, "Voltage sensor fault detection and reconfiguration for a doubly fed induction generator," in *Proc. IEEE Int. Symp. Diag. Electric Mach., Power Electron. Drives*, Sep. 2007, pp. 377–382.

[6] P. Poure, P. Weber, D. Theilliol, and S. Saadate, "Fault-tolerant power electronic converters: Reliability analysis of active power filter," in *Proc. IEEE Int. Symp. Ind. Electron.*, Jun. 2007, pp. 3174–3179.

[7] P. F. Odgaard, J. Stoustrup, and M. Kinnaert, "Fault tolerant control of wind turbines–A benchmark model," in *Proc. 7th IFAC Symp. Fault Detection, Supervis. Safety Tech. Int. Conf. Image Process.*, Jul. 2009, pp. 155–160.

[8] W. Chen, S. X. Ding, A. H. A. Sari, A. Naik, A. Q. Khan, and S. Yin, "Observer-based FDI schemes for wind turbine benchmark," in *Proc. IFAC World Congr.*, Aug.–Sep. 2011, pp. 7073–7078.

[9] N. Laouti, N. Sheibat-Othman, and S. Othman, "Support vector machines for fault detection in wind turbines," in *Proc. IFAC World Congr.*, Aug.–Sep. 2011, pp. 7067–7072.

[10] A. A. Ozdemir, P. Seiler, and G. J. Balas, "Wind turbine fault detection using counter-based residual thresholding," in *Proc. IFAC World Congr.*, Aug.–Sep. 2011, pp. 8289–8294.

[11] C. Svard and M. Nyberg, "Automated design of an FDI-system for the wind turbine benchmark," in *Proc. IFAC World Congr.*, Aug.–Sep. 2011, pp. 8307–8315.

[12] X. Zhang, Q. Zhang, S. Zhao, R. M. G. Ferrari, M. M. Polycarpou, and T. Parisini, "Fault detection and isolation of the wind turbine benchmark: An estimation-based approach," in *Proc. IFAC World Congr.*, Sep. 2011, pp. 8295–8300.

[13] P. Pisu and B. Ayalew, "Robust fault diagnosis for a horizontal axis wind turbine," in *Proc. IFAC World Congr.*, Aug.–Sep. 2011, pp. 7055–7060.

[14] J. Blesa, V. Puig, J. Romera, and J. Saludes, "Fault diagnosis of wind turbines using a set-membership approach," in *Proc. IFAC World Congr.*, Aug.–Sep. 2011, pp. 8316–8321.

[15] J. Dong and M. Verhaegen, "Data driven fault detection and isolation of a wind turbine benchmark," in *Proc. IFAC World Congr.*, Sep. 2011, pp. 7086–7091.

[16] F. Kiasi, J. Prakash, S. Shah, and J. M. Lee, "Fault detection and isolation of benchmark wind turbine using the likelihood ratio test," in *Proc. IFAC World Congr.*, Aug.–Sep. 2011, pp. 7079–7085.

[17] S. Simani, P. Castaldi, and M. Bonfe, "Hybrid model-based fault detection of wind turbine sensors," in *Proc. IFAC World Congr.*, Sep. 2011, pp. 7061–7066.

[18] S. Simani, P. Castaldi, and A. Tilli, "Data-driven approach for wind turbine actuator and sensor fault detection and isolation," in *Proc. IFAC World Congr.*, Aug.–Sep. 2011, pp. 8301–8306.

[19] F. Stoican, C.-F. Raduinea, and S. Olaru, "Adaptation of set theoretic methods to the fault detection of wind turbine benchmark," in *Proc. IFAC World Congr.*, Aug.–Sep. 2011, pp. 8322–8327.

[20] S. Simani and P. Castaldi, "Data–driven design of a fuzzy logic fault tolerant control for a wind turbine benchmark," in *Proc. Safeprocess*, Aug. 2012, pp. 108–113.

[21] D. Rotondo, F. Nejari, V. Puig, and J. Blesa, "Fault tolerant control of the wind turbine benchmark using virtual sensors/actuators," in *Proc. IFAC Safeprocess*, Aug. 2012, pp. 114–119.

[22] P. Casau, P. A. N. Rosa, S. Tabatabaeipour, and C. Silvestre, "Fault detection and isolation and fault tolerant control of wind turbines using set-valued observers," in *Proc. IFAC Safeprocess*, Aug. 2012, pp. 120–125.

[23] S. Simani and P. Castaldi, "Adaptive fault-tolerant control design approach for a wind turbine benchmark," in *Proc. IFAC Safeprocess*, Aug. 2012, pp. 319–324.

[24] M. Sami and R. Patton, "Global wind turbine FTC via T-S fuzzy modelling and control," in *Proc. IFAC Safeprocess*, Aug. 2012, pp. 325–330.

[25] M. Sami and R. Patton, "An FTC approach to wind turbine power maximisation via T-S fuzzy modelling and control," in *Proc. IFAC Safeprocess*, Aug. 2012, pp. 349–354.

[26] X. Yang and J. Maciejowski, "Fault-tolerant model predictive control of a wind turbine benchmark," in *Proc. IFAC Safeprocess*, Aug. 2012, pp. 337–342.

[27] J. Kim, I. Yang, and D. Lee, "Control allocation based compensation for faulty blade actuator of wind turbine," in *Proc. IFAC Safeprocess*, Aug. 2012, pp. 355–360.

[28] F.D. Bianchi, H. De Battista, and R. J. Mantz, *Wind Turbine Control Systems*. New York, NY, USA: Springer-Verlag, 2007.
[29] T. Burton, D. Sharpe, N. Jenkins, and E. Bossanyi, *Wind Energy Handbook*. 6 ed. New York, NY, USA: Wiley, 2008.
[30] I. Munteanu, A. I. Bratcu, N. A. Cutululis, and E. Caenga, *Optim. Control Wind Energy Syst. Toward Global Approach*, New York, NY, USA: Springer-Verlag, 2008.
[31] K. E. Johnson, M. J. Pao, L. Y. Balas, and L. J. Fingersh, "Control of variable-speed wind turbines-standard and adaptive techniques for maximizing energy capture," *IEEE Control Syst. Mag.*, vol. 26, no. 3, pp. 71–81, Jun. 2006.
[32] Z. Hameed, Y. S. Hong, Y. M. Cho, S. H. Ahn, and C. K. Song, "Condition monitoring and fault detection of wind turbines and related algorithms: A review," *Renew. Sustain. Energy Rev.*, vol. 13, no. 1, pp. 1–39, Jan. 2009.
[33] P. F. Odgaard, C. Damgaard, and R. Nielsen, "On-line estimation of wind turbine power coefficients using unknown input observers," in *Proc. 17th World Congr. Int. Fed. Autom. Control*, Jul. 2008, pp. 10646–10651.
[34] P.F. Odgaard, C. Damgaard, and R. Nielsen, "Adaptive power control of wind turbines based on power coefficient estimations," in *Proc. Eur. Wind Energy Conf.*, Apr. 2008, pp. 1–3.
[35] P. F. Odgaard, (2010). *Wind Turbine Benchmark Model for Fault Detection, Isolation and Accommodation* [Online]. Available: http://www.kk-electronic.com/wind-turbine-control/competition-on-fault-detection/wind-turbine-benchmark-model.aspx
[36] D. S. L. Dolan and P. W. Lehn, "Simulation model of wind turbine 3p torque oscillations due to wind shear and tower shadow," *IEEE Trans. Energy Convers.*, vol. 21, no. 3, pp. 717–724, Sep. 2006.
[37] T. Esbensen and C. Sloth, "Fault diagnosis and fault-tolerant control of wind turbines," M.S. thesis, Dept. Electroanal Eng., Aalborg Univ., Aalborg, Denmark, Jun. 2009.
[38] H. E. Merritt, *Hydraulic Control Systems*. New York, NY, USA: Wiley, 1967.
[39] X. Zhang, M. M. Polycarpou, and T. Parisini, "Design and analysis of a fault isolation scheme for a class of uncertain nonlinear systems," *IFAC Annu. Rev. Control*, vol. 3, no. 2, pp. 107–121, 2008.
[40] X. Zhang, M. M. Polycarpou, and T. Parisini, "A robust detection and isolation scheme for abrupt and incipient faults in nonlinear systems," *IEEE Trans. Autom. Control*, vol. 47, no. 4, pp. 576–593, Apr. 2002.
[41] C. Svard and M. Nyberg, "Residual generators for fault diagnosis using computation sequences with mixed causality applied to automotive systems," *IEEE Trans. Syst., Man Cybern., A, Syst. Humans*, vol. 40, no. 6, pp. 1310–1328, Nov. 2010.

Peter Fogh Odgaard (M'05) received the M.Sc. degree in electrical engineering and the Ph.D. degree in control engineering from Aalborg University, Aalborg, Denmark, in 2001 and 2004, respectively.

He was a Guest Researcher with the Department of Mathematics, Washington University, St. Louis, MO, USA, in 2003. From September 2004 to December 2006, he was a Research Assistant Professor with Aalborg University. From January 2007 to April 2013, he was a Control Specialist with kk-electronic a/s, Denmark. In April 2013, he joined Automation & Control, Aalborg University, as a Research Associate Professor. He has authored more than 60 peer-reviewed papers, and holds four patents and patent applications. His current research interests include control of wind turbines, wind farms and renewable energy generating systems, fault detection and isolation, fault tolerant control, model predictive control and wavelets.

Dr. Odgaard has been a member of IFAC Technical Committee SAFEPROCES and Power and Energy Systems since 2011. He has served as a Co-Chair of the Danish CSS/RAS joint chapter.

Jakob Stoustrup (SM'99) received the M.Sc. degree in electrical engineering and the Ph.D. degree in applied mathematics from the Department of Mathematics, Technical University of Denmark, Kongens Lyngby, Denmark.

He has held several positions with the Technical University of Denmark, as well as Visiting Professorships with the University of Strathclyde, Glasgow, U.K., and the Mittag-Leffler Institute, Djursholm, Sweden.

Dr. Stoustrup acted as an Associate Editor, Guest Editor, and Editorial Board member of several international journals. He is a former Chair of an IEEE chapter. Since 2008, he has been a Chairman for the IFAC Technical Committee SAFEPROCESS. He has been a member of IFAC Technical Board since 2011. He was a member of the Danish and Swedish Research Councils and the European Research Council. He was a Board member of The Danish Academy of Technical Sciences. His main contributions to robust control, fault tolerant control, and plug-and-play control have been made through 250-plus peer-reviewed papers. He has carried out industrial cooperation with approximately 100 companies.

Michel Kinnaert (M'10) graduated in mechanical and electrical engineering from Université libre de Bruxelles (ULB), Brussels, Belgium, in 1983. He received the M.S. degree in electrical engineering from Stanford University, Stanford, CA, USA, in 1984 and the Ph.D. degree from ULB, in 1987.

He was with the Belgian National Fund for Scientific Research. He was appointed by ULB, where he is currently a Professor with the Department of Control Engineering and System Analysis. He held two Visiting Professor positions at LAGEP, Université Claude Bernard Lyon 1, Lyon, France. He has co-authored, with M. Blanke, J. Lunze and M. Staroswiecki, the book *Diagnosis and Fault Tolerant Control* (2nd Ed., Springer, 2006). His current research interests include fault detection and isolation and fault tolerant control with applications to the process industries, power systems and mechatronic systems.

Dr. Kinnaert has been the Chairman of the IFAC Technical Committee, and he is an Associate Editor of Control Engineering Practice.